

Understanding $B \rightarrow D^{*-} N \bar{N}$ and Its Implications

Chun-Kiang Chua, Wei-Shu Hou and Shang-Yuu Tsai

Department of Physics, National Taiwan University, Taipei, Taiwan 10764, R.O.C.

(November 4, 2018)

The CLEO Collaboration recently reported the observation of the $B^0 \rightarrow D^{*-} p \bar{n}$ mode at a rate only a factor of 4–5 lower than $B^0 \rightarrow D^{*-} \rho^+$ and $D^{*-} \pi^+$. We try to understand this with a factorization approach of current produced nucleon pairs. The baryon weak vector current form factors are related by isospin rotation to nucleon electromagnetic form factors. By using $G_M^{p,n}$ measured from $e^+e^- \rightarrow \bar{N}N$ and $p\bar{p} \rightarrow e^+e^-$ processes, assuming factorization of the $B^0 \rightarrow D^{*-}$ transition and the $p\bar{n}$ pair production, we are able to account for up to 60% of the observed rate. The remainder is argued to arise from the axial current. The model is then applied to B decays to other mesons plus $p\bar{n}$ modes and D^{*-} plus strange baryon pairs.

PACS numbers: 13.25.Hw, 13.40.Gp, 14.20.Dh

I. INTRODUCTION

Following a suggestion by Dunietz [1] that $B \rightarrow DN\bar{X}$ decays could be sizable, the CLEO Collaboration has recently reported the first observation of such modes [2]:

$$\text{Br}(B^0 \rightarrow D^{*-} p \bar{n}) = (14.5_{-3.0}^{+3.4} \pm 2.7) \times 10^{-4}, \quad (1)$$

$$\text{Br}(B^0 \rightarrow D^{*-} p \bar{p} \pi^+) = (6.5_{-1.2}^{+1.3} \pm 1.0) \times 10^{-4}. \quad (2)$$

Although the decay final states are three or four-body, they are only a few times below corresponding two-body mesonic modes [3] such as

$$\text{Br}(B^0 \rightarrow D^{*-} \rho^+) = (6.8 \pm 3.4) \times 10^{-3}, \quad (3)$$

$$\text{Br}(B^0 \rightarrow D^{*-} \pi^+) = (2.76 \pm 0.21) \times 10^{-3}. \quad (4)$$

Since D^{*-} creation carries away much energy, the observed large rate of $B^0 \rightarrow D^{*-} p \bar{n}$ supports the suggestion that enhanced baryon production is favored by reduced energy release on the baryon side [4]. Thus, given the large rate of $B \rightarrow \eta' + X_s$ decay where $p_{\eta'} > 2$ GeV [5], the $B \rightarrow \eta' \Lambda \bar{p}$ decay may be sizable [4] compared to charmless two body baryonic modes. Similar argument holds for $B \rightarrow \gamma \Lambda \bar{p}$ as implied by $B \rightarrow \gamma + X_s$. Since $\Lambda \rightarrow p\pi$ decay automatically provides spin information, the observation of such charmless three (or more) body baryonic modes involving Λ baryons allows for a search program for triple-product type of CP and T violating effects. With this in mind, a better understanding of the $B^0 \rightarrow D^{*-} p \bar{n}$ decay is not only worthwhile in its own right, it can also serve as an important first step towards a more ambitious project on charmless baryonic modes.

In order to account for the proximity of rates shown in Eqs. (1) and (3), $B^0 \rightarrow D^{*-} p \bar{n}$ was seen through a simple pole model [4] as occurring in two steps of an underlying $\bar{b} \rightarrow \bar{c} u \bar{d}$ transition, i.e. $B \rightarrow D^{*-} h$ followed by $h \rightarrow N \bar{N}$, where h stands for the off-shell π^+ and ρ^+ mesons, as illustrated in Fig. 1(a). Taking this as a Feynman diagram, the decay amplitude of $B^0 \rightarrow D^{*-} p \bar{n}$ can be written as

$$i\mathcal{M}_\rho = \left(-i \frac{G_F}{\sqrt{2}} V_{ud} V_{cb}^* a_1 \right) \langle D^{*-} | V_\mu - A_\mu | B^0 \rangle \\ \times f_\rho m_\rho \times i \left(\frac{-g^{\mu\lambda} + \frac{q^\mu q^\lambda}{m_\rho^2}}{q^2 - m_\rho^2} \right) \\ \times i\sqrt{2} \bar{u}(p_p) \left[g_1^{\rho N \bar{N}} \gamma_\lambda + \frac{i g_2^{\rho N \bar{N}}}{2m_N} \sigma_{\lambda\xi} q^\xi \right] v(p_{\bar{n}}), \quad (5)$$

where the $B^0 \rightarrow D^{*-}$ transition matrix element is

$$\langle D^{*-} | V_\mu - A_\mu | B^0 \rangle = \left[-\epsilon_{\mu\nu\alpha\beta} p_B^\alpha p_{D^*}^\beta \frac{2V(q^2)}{m_B + m_{D^*}} \right. \\ -i \left(g_{\mu\nu} - \frac{q_\mu q_\nu}{q^2} \right) (m_B + m_{D^*}) A_1(q^2) \\ \left. + i \left((p_B + p_{D^*})_\mu - \frac{m_B^2 - m_{D^*}^2}{q^2} q_\mu \right) \frac{A_2(q^2)}{m_B + m_{D^*}} q_\nu \right. \\ \left. -i 2m_{D^*} \frac{q_\mu q_\nu}{q^2} A_0(q^2) \right] \epsilon_{D^*}^{\nu\mu}, \quad (6)$$

$q = p_B - p_{D^*} = p_p + p_{\bar{n}}$ is the momentum transfer (so $t = q^2$ is nothing but the $p\bar{n}$ pair mass), ϵ_{D^*} is the polarization of the D^{*-} meson, and $g_1^{\rho N \bar{N}}$ and $g_2^{\rho N \bar{N}}$ are respectively the vector (Dirac) and tensor (Pauli) coupling constants of the ρ -meson to the nucleons.

In Eq. (5), factorization of the first vertex is justified to some extent, and is expressed through the effective coefficient a_1 . For example, in “naive factorization”, $a_1 = c_1 + c_2/N_c$ where N_c is the number of quark colors and $c_{1,2}$ are Wilson coefficients, but in general the

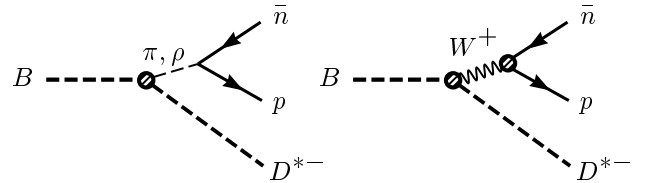


FIG. 1. (a) The simple pole model and (b) the factorized current model for describing $B^0 \rightarrow D^{*-} p \bar{n}$.

effective coefficient a_1 can be extracted from experimental data on $B^0 \rightarrow D^{*-}\rho^+$ decay. The problem of the pole model picture is with single ρ dominance and the q^2 dependence of the strong interaction $\rho N\bar{N}$ vertex. That is, there is no reason why the $u\bar{d}$ weak current only generates a ρ meson, which then propagates and generates the baryon pair, as seen from the second and third lines of Eq. (5). Quantitative results based on this model is highly unreliable, which is further aggravated by our ignorance of time-like meson-nucleon couplings. Since our knowledge of the coupling $g_1^{\rho N\bar{N}}$ are based on low $Q^2(\equiv -q^2)$ space-like processes, they cannot be expected to give reliable quantitative results for time-like processes at higher energies.

In this paper we turn to a different approach by proposing a generalized factorization of current produced $p\bar{n}$ pairs. The three-body decay is seen as generated by two factorized weak currents (linked by a W -boson), where one current converts B^0 into D^{*-} and the other creates the $p\bar{n}$ pair, as shown in Fig. 1(b). In this way, having factorized the $B^0 \rightarrow D^{*-}$ transition, we concentrate on the weak current production of baryon pairs.

It is well known that the vector portion of the weak current and the isovector component of the electromagnetic (em) current form an isotriplet. Thus, information on the nucleon em form factors, for which much data exist in both the space-like region [6] (e.g. $ep \rightarrow ep$), and, of particular interest to us, the time-like region [7–10] (e.g. $e^+e^- \rightarrow N\bar{N}$ and $p\bar{p} \rightarrow e^+e^-$), can be transferred to the nucleon weak form factors by a simple isospin rotation. The total decay amplitude that comes from the vector portion of the weak current can be written down unambiguously and the portion of the branching fraction that comes solely from the weak vector current can be readily obtained once the form factors are given. We find that the vector current can account for 50%–60% of the observed rate of Eq. (1). Since this analysis involves just the factorization hypothesis but is otherwise based on data, it is rather robust.

Although the axial vector and vector current contributions interfere in the decay amplitude, the interference vanishes when one sums over spin and integrates over phase space. The total rate is therefore a simple sum of the contributions from the vector and axial vector portions of the weak nucleon form factor. Like the vector case, we could in principle obtain the axial vector contribution if the nucleon form factors of the axial current were known. Unfortunately, the time-like data is still lacking, hence the contribution from this part remains undetermined. In spite of this, a rough estimate can still be given, which seems to be the right amount. We point out, however, that information on the time-like *nucleon* axial form factor could in fact be obtained in the future via the $B^0 \rightarrow D^{*-}p\bar{n}$ decay data. One just has to separate the axial vector contribution from the vector part.

This paper is organized as follows: in the next section we lay out the factorization assumption that allows us

to relate the vector current contribution to the nucleon em form factors, where one enjoys abundance of experimental data. We are then able to compute the vector current contribution to $B^0 \rightarrow D^{*-}p\bar{n}$. The axial vector contribution is also estimated. In Sec. III, to illustrate the power of our data based approach, we briefly introduce an improved pole model approach and stress the need for improved measurements of neutron em form factors. Finally, we apply our analysis to $B^+ \rightarrow \bar{D}^{(*)0}p\bar{n}$ and $B^0 \rightarrow D^-p\bar{n}$ and other baryonic modes containing strangeness, and conclude in the last section.

II. FACTORIZATION APPROACH AND NUCLEON FORM FACTOR DATA

As illustrated in Fig. 1(b), we generalize factorization from two-body to three-body decay processes,

$$\langle D^{*-}p\bar{n} | \mathcal{H}_{eff} | B^0 \rangle = \frac{G_F}{\sqrt{2}} V_{ud} V_{cb}^* a_1 \langle D^{*-} | V^\mu - A^\mu | B^0 \rangle \times \langle p\bar{n} | V_\mu - A_\mu | 0 \rangle. \quad (7)$$

The first matrix element is as before, but for the second, the nucleon pair is viewed as directly created by the current. The vector part can be expressed as

$$\langle p\bar{n} | V_\mu | 0 \rangle = \bar{u}(p_p) \left\{ F_1^W(t) \gamma_\mu + i \frac{F_2^W(t)}{2m_N} \sigma_{\mu\nu} q^\nu \right\} v(p_{\bar{n}}), \quad (8)$$

where m_N is the nucleon mass, $t \equiv (p_p + p_{\bar{n}})^2 = q^2$, and $F_{1,2}^W$ are the weak nucleon form factors. Likewise, the weak axial current $A_\mu \equiv A_\mu^1 + iA_\mu^2$ matrix element is

$$\langle p\bar{n} | A_\mu | 0 \rangle = \bar{u}(p_p) \left\{ g_A(t) \gamma_\mu + \frac{h_A(t)}{2m_N} q_\mu \right\} \gamma_5 v(p_{\bar{n}}), \quad (9)$$

where $g_A(t)$ is the axial form factor, and $h_A(t)$ is referred to as the induced pseudoscalar form factor. Expressions for the space-like processes are similar. The weak nucleon form factor $F_1^W(t)$ and the axial form factor $g_A(t)$ are normalized at $t = 0$ [3]

$$F_1^W(0) = 1, \quad g_A(0) \equiv g_A = 1.2670 \pm 0.0035. \quad (10)$$

A. Isospin Relation and Nucleon Form Factors

It is well known that the photon field A_μ contains W_μ^3 , which forms a weak isotriplet with $W_\mu^{1,2}$. Therefore the currents they couple to also form an isotriplet, and are related by an isospin transformation. For the nucleon system, the strong isospin symmetry coincides with the weak isospin symmetry of the weak and em currents. The

weak vector form factors are therefore related to isovector electromagnetic (em) form factors.

The matrix element $\langle N(p')\bar{N}(p)|\mathcal{J}_\mu^{em}|0\rangle$ for the em current can be expressed as

$$\begin{aligned} & \langle N(p')\bar{N}(p)|\mathcal{J}_\mu^{em}|0\rangle \\ &= \bar{u}(p')\left\{F_1(t)\gamma_\mu + i\frac{F_2(t)}{2m_N}\sigma_{\mu\nu}q^\nu\right\}v(p). \end{aligned} \quad (11)$$

Similar expressions can be obtained for space-like processes. The quantities $F_1(t)$, $F_2(t)$ are respectively the Dirac and Pauli form factors, normalized at $t=0$ as

$$F_1^p(0) = 1, \quad F_1^n(0) = 0, \quad F_2^p(0) = \kappa_p, \quad F_2^n(0) = \kappa_n, \quad (12)$$

with κ_p (κ_n) the proton (neutron) anomalous magnetic moment in nuclear magneton units. The experimental data is usually given in terms of the Sachs form factors, which are related to F_1 and F_2 through

$$\begin{aligned} G_E^{p,n}(t) &= F_1^{p,n}(t) + \frac{t}{4m_N^2}F_2^{p,n}(t), \\ G_M^{p,n}(t) &= F_1^{p,n}(t) + F_2^{p,n}(t). \end{aligned} \quad (13)$$

One clearly has $G_M = G_E$ at threshold $t = 4m_N^2$, while at $t=0$ we have

$$G_E^p(0) = 1, \quad G_E^n(0) = 0, \quad G_M^p(0) = 1 + \kappa_p, \quad G_M^n(0) = \kappa_n. \quad (14)$$

The isospin decomposition of the em current is given by the following definitions

$$F_i^{s,v} = \frac{1}{2}(F_i^p \pm F_i^n), \quad (i = 1, 2), \quad (15)$$

where F_i^s and F_i^v are the isoscalar and isovector decompositions of the form factors, respectively. The fact that the isovector component of the em current, together with the vector portion of the charged weak currents, form an isotriplet is manifested by

$$2F_i^v(t) = F_i^W(t), \quad i = 1, 2, \quad (16)$$

the factor 2 coming from the definition of $F_{1,2}^{(s,v)}(t)$ in Eq. (15). For example, from Eqs. (10), (12) and (15) we have $2F_1^v(0) = F_1^W(0)$.

With Eq. (16) and the Gordon decomposition, we can put the three-body $B^0 \rightarrow D^{*-}p\bar{n}$ decay amplitude of Eq. (8) into the following form

$$\begin{aligned} i\mathcal{M}_V &= -i\frac{G_F}{\sqrt{2}}V_{ud}V_{cb}^*a_1\epsilon_{D^*}^{\nu\mu}\left[-\epsilon_{\mu\nu\alpha\beta}p_B^\alpha p_{D^*}^\beta\frac{2V(q^2)}{m_B+m_{D^*}}\right. \\ &\quad \left.-ig_{\mu\nu}(m_B+m_{D^*})A_1(q^2) + i(p_B+p_{D^*})_\mu q_\nu\frac{A_2(q^2)}{m_B+m_{D^*}}\right] \\ &\quad \times \bar{u}(p_p)\left[2(F_1^v+F_2^v)\gamma^\mu + \frac{F_2^v}{m_N}(p_{\bar{n}}-p_p)^\mu\right]v(p_{\bar{n}}), \end{aligned} \quad (17)$$

where V indicates that the nucleon pair is generated by the vector current. The terms proportional to q_μ in Eq. (6) vanish in the limit of equal proton and neutron mass. For completeness, the amplitude for nucleons generated by the axial vector current is given by

$$\begin{aligned} i\mathcal{M}_A &= -i\frac{G_F}{\sqrt{2}}V_{ud}V_{cb}^*a_1\langle D^{*-}|V_\mu - A_\mu|B^0\rangle \\ &\quad \times \bar{u}(p_p)\left[g_A(t)\gamma^\mu\gamma_5 + \frac{h_A(t)}{2m_N}q^\mu\gamma_5\right]v(p_{\bar{n}}), \end{aligned} \quad (18)$$

where $\langle D^{*-}|V_\mu - A_\mu|B^0\rangle$ is given in Eq. (6).

The two amplitudes \mathcal{M}_A and \mathcal{M}_V interfere, since

$$\begin{aligned} \sum 2\text{Re}(\mathcal{M}_A\mathcal{M}_V^*) &= 32G_F^2|V_{ud}|^2|V_{cb}|^2a_1^2 \\ &\quad \times g_A(t)V(t)A_1(t)\left(G_M^p(t) - G_M^n(t)\right) \\ &\quad \times \left[(p_B \cdot p_p)(p_{D^*} \cdot p_{\bar{n}}) - (p_{D^*} \cdot p_p)(p_B \cdot p_{\bar{n}})\right] \end{aligned} \quad (19)$$

is in general non-vanishing. The summation is performed over the nucleon spins and D^{*-} polarization. The three-body phase space is described by the two independent variables $m_{p\bar{n}}^2 \equiv t = (p_p + p_{\bar{n}})^2$ and $m_{D^*\bar{n}}^2 \equiv (p_{D^*} + p_{\bar{n}})^2$. The interference term is antisymmetric with respect to exchange of p_p and $p_{\bar{n}}$. For given t , as we integrate over the kinematically allowed $m_{D^*\bar{n}}^2$, each value of $\sum 2\text{Re}(\mathcal{M}_A\mathcal{M}_V^*)$ from a given pair of $p_p, p_{\bar{n}}$ would be cancelled by those from the exchanged pair. The interference term thus contributes nothing to the total three body decay rate Γ , and the final result is a simple sum of the contribution from \mathcal{M}_V and \mathcal{M}_A separately.

It is interesting to note that, although the effect of $\sum 2\text{Re}(\mathcal{M}_A\mathcal{M}_V^*)$ does not show up in the decay rate, we can nevertheless construct an asymmetry ratio measurable based on the antisymmetric nature of this quantity, to extract the time-like information of $g_A(t)$ from $B^0 \rightarrow D^{*-}p\bar{n}$ data. The information of $V(t)$, $A_1(t)$ and $G_M^{p,n}(t)$ in Eq. (19) can be found by other means, and the overall factors a_1 and $|V_{ud}|, |V_{cb}|$ would cancel in the asymmetry ratio.

B. Form Factor Data and Perturbative QCD

Much data has been accumulated for the nucleon em form factors, which turns the vector portion of the decay amplitude $i\mathcal{M}_V$ expressed in Eq. (17) into something that we can handle. The branching fraction can be readily obtained once the nucleon em form factors are given, thanks to the isospin relation of weak vector and em currents. It is important, however, to make sure that the form factors satisfy the constraint from perturbative QCD (PQCD).

The so-called quark counting rules [11] give the leading power in the large- $|t|$ fall-off of the form factor $F_1(t)$ by counting the number of gluon exchanges which are

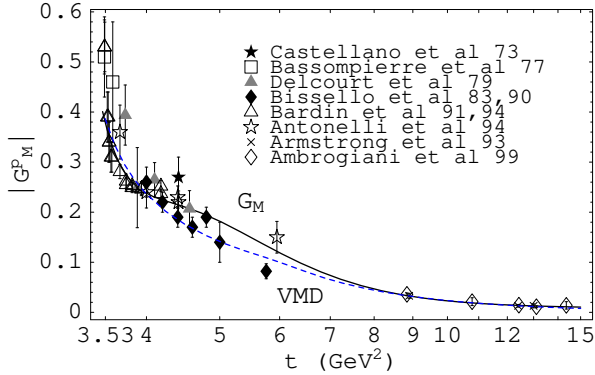


FIG. 2. Time-like proton magnetic form factor data, fitted (solid) by Eq. (22) with the parameters given in Eq. (24). The other (dash) curve is discussed in Sec. III.

necessary to distribute the large photon momentum to all constituents. Since helicity-flip leads to an extra $1/t$ factor in $F_2(t)$, one finds, in the limit $|t| \rightarrow \infty$

$$F_i(t) \rightarrow (|t|)^{-(i+1)} \left[\ln \left(\frac{|t|}{Q_0^2} \right) \right]^{-\gamma}, \quad \gamma = 2 + \frac{4}{3\beta},$$

$$i = 1, 2 \quad (20)$$

where β is the β -function of QCD to one loop, and $Q_0 \simeq \Lambda_{\text{QCD}} = 0.3 \text{ GeV}$. We note that γ depends weakly on the number of flavors; for three flavors $\gamma = 2.148$.

The asymptotic form given in Eq. (20) has been confirmed by many experimental measurements of $G_M = F_1 + F_2$ over a wide range of momentum transfers in the space-like region. The asymptotic behavior for G_M^p also seems to hold in the time-like region, as reported by the Fermilab E760 experiment [9] for $8.9 \text{ GeV}^2 < t < 13 \text{ GeV}^2$. Another Fermilab experiment, E835, has recently reported G_M^p for momentum transfer up to $\sim 14.4 \text{ GeV}^2$, and gives the empirical fit [7]:

$$|G_M^p| = \frac{C}{t^2 \left[\ln \left(\frac{t}{Q_0^2} \right) \right]^2}, \quad (21)$$

which agrees well with the asymptotic form in Eq. (20).

By exploiting the relation in Eq. (13), the combination $2(F_1^v + F_2^v)$ in Eq. (17) can be replaced by $G_M^p - G_M^n$ which is composed of measurable quantities. Similar replacement can also be made for F_2 , which is a combination of $G_M^p - G_E^p$ and $G_M^n - G_E^n$. Most time-like data for the magnetic form factors, however, are extracted by assuming either $|G_E| = |G_M|$ or $|G_E| = 0$ in the region of momentum transfer explored. Since $G_M - G_E = (1 - t/4m_N^2)F_2$ clearly vanishes at threshold, the absence of clear deviation from this assumption in extracting data implies the contribution of F_2 is negligible even for t far beyond the threshold, which is consistent with the prediction from QCD. In fact, by assuming $|G_E| = |G_M|$ in extracting

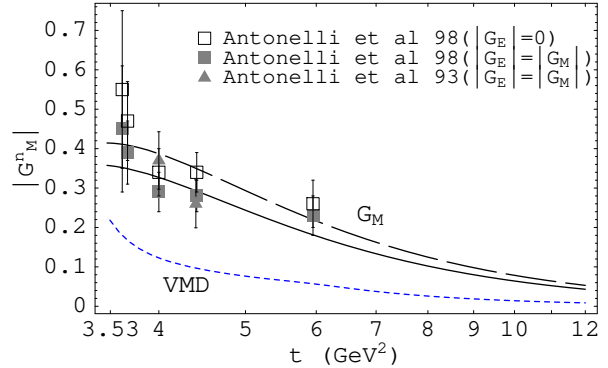


FIG. 3. Time-like neutron magnetic form factor, where solid (long dash) line is fitted by Eq. (23) with parameters given in Eq. (25) (Eq. (26)), for data extracted with $|G_E| = |G_M|$ ($|G_E| = 0$) assumption. The third (dash) curve is discussed in Sec. III.

G_M from data, the information on F_2 is lost. In our calculation we concentrate on the part of Eq. (17) which contains $F_1^v + F_2^v$. The contribution from F_2^v can be determined only when G_M and G_E can be separated from data with better angular resolution.

We take $|G_M|$ in the following form to make a *phenomenological fit* of the experimental data [7–10]:

$$|G_M^p(t)| = \left(\frac{x_1}{t^2} + \frac{x_2}{t^3} + \frac{x_3}{t^4} + \frac{x_4}{t^5} + \frac{x_5}{t^6} \right) \left[\ln \left(\frac{t}{Q_0^2} \right) \right]^{-\gamma}, \quad (22)$$

$$|G_M^n(t)| = \left(\frac{y_1}{t^2} + \frac{y_2}{t^3} \right) \left[\ln \left(\frac{t}{Q_0^2} \right) \right]^{-\gamma}, \quad (23)$$

where the leading power and log factor are from Eq. (20), and the fewer parameters for G_M^n reflects the scarcer amount of neutron data. We find the best fit values

$$\begin{aligned} x_1 &= 420.96 \text{ GeV}^4, & x_4 &= -433916.61 \text{ GeV}^{10}, \\ x_2 &= -10485.50 \text{ GeV}^6, & x_5 &= 613780.15 \text{ GeV}^{12}, \\ x_3 &= 106390.97 \text{ GeV}^8, \end{aligned} \quad (24)$$

and

$$y_1 = 236.69 \text{ GeV}^4, \quad y_2 = -579.51 \text{ GeV}^6, \quad (25)$$

where the χ^2 per degree of freedom of the fits are 1.47, 0.41 for $|G_M^p|$, $|G_M^n|$, respectively. We show in Figs. 2 and 3 the fitted data together with the best fit curves given by Eq. (22) and (23) with the parameters above.

It was pointed out in Ref. [8] that the data supports $|G_E^n| = 0$ as well. We therefore perform the fit for the neutron magnetic form factor to the data that is extracted under the assumption of $|G_E^n| = 0$. Since the

number of data points is small, a two-parameter fit as in Eq. (23) would still suffice. The best fit values are

$$y_1 = 292.62 \text{ GeV}^4, \quad y_2 = -735.73 \text{ GeV}^6, \quad (26)$$

giving $\chi^2/\text{d.o.f.} = 0.39$, which is a little smaller than the previous fit, and the fit is plotted as the long-dashed line in Fig. 3. To the eye, the data might slightly prefer the second fit, especially the $t = 6 \text{ GeV}^2$ data point. However, it should be clear that more data is needed to distinguish between these two cases.

We note that there is a sign difference between G_M^p and G_M^n in the space-like region, since from Eq. (14) $G_M^p(0) = 1 + \kappa_p > 0$ and $G_M^n(0) = \kappa_n < 0$. Analyticity implies continuity at infinity between space-like and time-like t [12] regions. Hence time-like magnetic form factors are expected to behave like space-like magnetic form factors, i.e. real and positive for the proton, but negative for the neutron.

For large t , QCD predicts the magnetic form factors to be real [11], with the neutron form factor weaker than the proton case [13]. According to QCD sum rules [14], asymptotically one expects $G_M^n/G_M^p \sim Q_d/Q_u = -0.5$. We can readily check our fits against these: for G_M fitted to data extracted by assuming $|G_E| = |G_M|$ for both neutron and proton magnetic form factors, we have $G_M^n/G_M^p = -y_1/x_1 = -236.69/420.96 = -0.56 \sim -0.5$. For G_M fitted to the proton data extracted with the assumption $|G_E| = |G_M|$ but the neutron data extracted assuming $|G_E| = 0$, we have $G_M^n/G_M^p = -y_1/x_1 = -292.62/420.96 = -0.70$, slightly larger than -0.5 . Nucleon form factors have also been analyzed from negative to positive t with dispersion relations. The phase of the proton magnetic form factor turns out to be $\sim 2\pi$, hence the proton magnetic form factor is real and positive as expected asymptotically, but already from $t \geq 4 \text{ GeV}^2$ [15,16] onwards.

C. Results for $B^0 \rightarrow D^{*-} p \bar{n}$

Before using data and the nucleon form factor relations to compute the decay rate, we need to specify the value of a_1 to be used. Since Eq. (17) depends on the product of a_1 and $B \rightarrow D^* \rho^+$ form factors [17], we take a phenomenological approach and use the value of a_1 extracted from the two-body mode $B \rightarrow D^{*-} \rho^+$, i.e. $a_1^{\text{BSW}} = 0.86 \pm 0.21 \pm 0.07$ and $a_1^{\text{LF}} = 0.74 \pm 0.18 \pm 0.06$ for Bauer-Stech-Wirbel (BSW) [18,19] and light-front (LF) form factor models [20]. The CKM matrix elements V_{ud} and V_{cb} are taken to be 0.9757, 0.039 respectively.

For both proton and neutron data extracted by assuming $|G_E| = |G_M|$, the predicted branching ratios are

$$\text{Br}_V^{\text{LF}} = (7.14_{-0.65}^{+0.69}) \times 10^{-4} \left(\frac{a_1}{0.74} \right)^2, \quad (27)$$

for the light-front (LF) model, and

$$\text{Br}_V^{\text{BSW}} = (8.72_{-0.79}^{+0.85}) \times 10^{-4} \left(\frac{a_1}{0.86} \right)^2, \quad (28)$$

for the BSW model. The subscript V serves as a reminder that this is the result from the vector portion of the weak current alone. The upper and lower errors correspond respectively to the maximum and minimum of the branching fraction evaluated by scanning through both $\chi^2 \leq \chi_{\text{min}}^2 + 1$ of $|G_M^p|$ and $|G_M^n|$ fits.

For proton data extracted by assuming $|G_E^p| = |G_M^p|$ but neutron data assuming $|G_E^n| = 0$, we have

$$\text{Br}_V^{\text{LF}} = (8.96_{-0.94}^{+1.02}) \times 10^{-4} \left(\frac{a_1}{0.74} \right)^2, \quad (29)$$

$$\text{Br}_V^{\text{BSW}} = (10.94_{-1.15}^{+1.25}) \times 10^{-4} \left(\frac{a_1}{0.86} \right)^2. \quad (30)$$

The larger values for this second set of branching fractions can be understood qualitatively from Fig. 3, where the curve fitted to data assuming $|G_E| = 0$ is higher than the one fitted assuming $|G_E| = |G_M|$. Since the neutron magnetic form factor is negative in the time-like region, the quantity $G_M^p - G_M^n$ is larger if G_M^n gets more negative, and the branching fraction becomes larger.

Comparing with the central value of the measured $\text{Br}(B^0 \rightarrow D^{*-} p \bar{n}) = (14.5_{-3.0}^{+3.4} \pm 2.7) \times 10^{-4}$, our LF (BSW) model results contribute 50 (60)% for the first set and 62 (75)% for the second. If the naive factorization value for a_1 is used, the results are close to the experimental central value, that is $\text{Br}_V^{\text{LF(BSW)}} = 12.51$ (13.83) $\times 10^{-4}$ for the first set and 15.69 (17.36) $\times 10^{-4}$ for the second set. We plot in Fig. 4 the vector current induced differential decay rate $d\Gamma_V(B^0 \rightarrow D^{*-} p \bar{n})/dq^2$, for both the LF and the BSW models. The lower two curves are from the approach of next section. As seen also from Eqs. (27-30), the LF form factor model gives results that

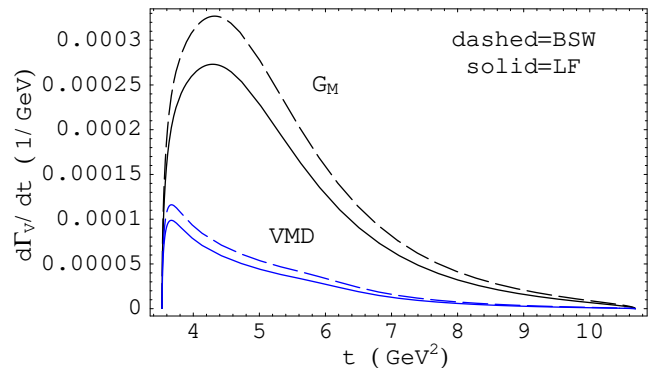


FIG. 4. The differential decay rate vs $t = m_{p\bar{n}}^2$ of the vector current induced $B^0 \rightarrow D^{*-} p \bar{n}$ decay. The upper curves are from the phenomenological fits to nucleon form factor data assuming $|G_E| = |G_M|$, for the Light-Front (solid) and BSW (dashed) $B^0 \rightarrow D^{*-}$ form factor models. The lower curves are for the VMD model discussed in the next section.

are smaller than the BSW model case. The $\sim 10\%$ difference can be viewed as an estimate of the uncertainty from $B \rightarrow D^*$ form factor models.

From Fig. 4 we see that the differential rate peaks at $\sim 4.6 \text{ GeV}^2$, corresponding to $m_{p\bar{n}} \simeq 2.14 \text{ GeV}$, which is quite close to the threshold of 1.88 GeV . This threshold enhancement effect, consistent with what was suggested in Ref. [4], should be checked experimentally by measuring the recoil D^{*-} momentum spectrum.

D. Estimate of Axial Current Contribution

Although the time-like data for the form factors of the axial current is still lacking, we can nevertheless make a rough estimate of its contribution. In analogy with the nucleon em form factors which are constrained by the asymptotic form of Eq. (20), we expect that, for large t , $g_A(t)$ behaves as $1/t^2$ and dominates over $h_A(t)$, which behaves like $1/t^3$. Taking cue from the similarity between Eqs. (17) and (18), we estimate the axial vector contribution by making a simple comparison and scaling from the vector case. Since we only have space-like information for the $g_A(t)$ form factor, we estimate $g_A(t_{\text{th}})$ at threshold by assuming same threshold enhancement factor as the $G_M^p(t) - G_M^n(t)$ case.

With this and Eqs. (17) and (18) in mind, to estimate the axial vector current contribution, we scale the decay rate obtained from the vector case by the ratio $g_A^2(-t_{\text{th}})/(G_M^p(-t_{\text{th}}) - G_M^n(-t_{\text{th}}))^2$ for space-like momentum. We use a dipole fit $g_A(t) = g_A(0)/(1 - t/M_A^2)^2$ with the axial mass $M_A = 1.077 \pm 0.039 \text{ GeV}$ [21]. For $t = -4m_N^2$, the ratio $r(t) \equiv g_A(t)/(G_M^p(t) - G_M^n(t))$ gives $r(-4m_N^2) \sim 0.59$. Assuming this ratio holds also at the threshold $t = 4m_N^2$, then $r^2(4m_N^2) \sim 0.35$ could be taken as the ratio of the branching fraction from the weak axial vector current to that from the weak vector current, i.e. $\text{Br}_A/\text{Br}_V \sim r^2(4m_N^2)$. For the results from fitting data assuming $|G_E| = |G_M|$, the total rate $\text{Br} = \text{Br}_V + \text{Br}_A$ would then be $\text{Br}^{\text{LF}} \sim (1 + 0.35) \times (7.14 \times 10^{-4}) = 9.64 \times 10^{-4}$ and $\text{Br}^{\text{BSW}} \sim 11.77 \times 10^{-4}$. On the other hand, for the results from fitting data assuming $|G_E| = 0$, the total rate would be $\text{Br}^{\text{LF}} \sim (1 + 0.35) \times (8.96 \times 10^{-4}) = 12.10 \times 10^{-4}$ and $\text{Br}^{\text{BSW}} \sim 14.77 \times 10^{-4}$, quite compatible with the experimental value of $(14.5_{-3.0}^{+3.4} \pm 2.7) \times 10^{-4}$. Another value of t which could be of interest is $t = 0$. Assuming that the ratio $r(0) \sim 0.27$ holds at threshold, then from $r^2(0) \sim 0.07 \sim \text{Br}_A/\text{Br}_V$, the total rate $\text{Br} = \text{Br}_V + \text{Br}_A$ is dominated by the vector current contribution.

To improve our result, we urge for more experimental measurements of $G_M^n(t)$, $G_E^{p,n}(t)$ and $g_A(t)$. In turn, if the predictions (strength and spectrum) from our model based on the vector part are confirmed by experiment, the measurements of $B \rightarrow \bar{D}^* p \bar{n}$ could provide useful feedback on nucleon axial form factors.

III. INTERRELATION WITH NUCLEON FORM FACTOR MODELS

The nucleon form factor is one of the oldest subjects in particle physics. It has provided us with a wealth of information and insight, and remains an active field to this date. In the preceding section, we made a simple phenomenological fit of nucleon em form factor data, then used an isospin relation and a factorization hypothesis to compute the $B^0 \rightarrow D^{*-} p \bar{n}$ rate, with some success. Although we made use of PQCD counting rules, we did not utilize tools such as analyticity. On the other hand, we mentioned the possibility that $B^0 \rightarrow D^{*-} p \bar{n}$ type of modes could eventually provide useful information on the nucleon form factor itself.

To exploit the utility of analyticity and to illustrate future interrelations between $B^0 \rightarrow D^{*-} p \bar{n}$ and nucleon form factors, we adopt a specific nucleon form factor model and discuss where it may be improved. The discussion would also shed some light on form factor decompositions, as well as the possible approach to $B \rightarrow \gamma p \bar{\Lambda}$, $\eta' p \bar{\Lambda}$ modes, which we shall briefly touch upon later.

A. Dispersion Analysis and VMD Hypothesis

Among the various approaches to the nucleon em form factors, of particular interest is the Vector-Meson-Dominance (VMD) hypothesis, which states that a photon couples to the hadrons via intermediate vector mesons such as ρ , ω , ϕ , etc. The simple pole model of Fig. 1(a) is a limited form of the VMD hypothesis. In Ref. [22], a parameterization of the nucleon em form factors based on dispersion analysis was proposed, which is constrained by several physical conditions, including PQCD power counting. The starting point is the dispersion relation

$$F(t) = \frac{1}{\pi} \int_{t_0}^{\infty} \frac{\text{Im} F(t')}{t' - t} dt', \quad (31)$$

where $F(t)$ stands for the nucleon em form factors $F_{1,2}^v(t)$. To gain predictive power, one truncates the spectral function by a few vector meson poles, where, to mimic the effect of large t continuum and to enforce PQCD counting rules, a fictitious pole is introduced. Thus, the form factors take the form

$$F_i^v(t) = \sum_v \frac{a_i^v}{M_v^2 - t}, \quad i = 1, 2, \quad (32)$$

where $a_{1,2}^v$ are related to the vector ($i = 1$) and tensor ($i = 2$) coupling constants of Eq. (5) via

$$\sqrt{2} a_i^v = m_v f_v g_i^{vNN}, \quad (33)$$

and f_v is the vector meson decay constant. This clearly extends the simple ρ meson exchange picture. Together

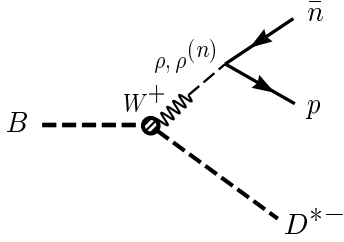


FIG. 5. The VMD picture for $B^0 \rightarrow D^{*-} p \bar{n}$ decay. The W boson couples to the nucleon pair via vector mesons which in our case are ρ and three excited states, including a fictitious pole to mimic continuum effect.

with our factorization ansatz, the $B^0 \rightarrow D^{*-} p \bar{n}$ transition can be pictured as in Fig. 5.

Following Ref. [22] we now consider the following parameterization of the form factors:

$$F_i^v(t) = \left[\tilde{F}_i^\rho(t) + \sum_v \frac{a_i^v L^{-1}(M_v^2)}{M_v^2 - t} \right] L(t), \quad (34)$$

where

$$L(t) \equiv \left[\ln \left(\frac{\Lambda^2 - t}{Q_1^2} \right) \right]^{-\gamma}, \quad (35)$$

$$\tilde{F}_i^\rho(t) = \frac{a_i^\rho L^{-1}(M_a^2) + b_i^\rho L^{-1}(M_b^2) (1 - t/c_i^\rho)^{-2/i}}{2(1 - t/d_i^\rho)}, \quad (36)$$

for $i = 1, 2$, where $a_1^\rho = 1.0317$, $a_2^\rho = 5.7824$, $b_1^\rho = 0.0875$, $b_2^\rho = 0.3907$, $c_1^\rho = 0.3176$, $c_2^\rho = 0.1422$, $d_1^\rho = 0.5496$, $d_2^\rho = 0.5362$, and $M_a^2 = 0.5 \text{ GeV}^2$, $M_b^2 = 0.4 \text{ GeV}^2$. Since the form factors also receive constraints from perturbative QCD for large momentum transfer, a logarithmic factor, Eq. (35), is given for consistency. Apart from this, Eq. (34) contains two terms: $\tilde{F}_i^\rho(t)$ represents the 2π -continuum plus the ρ pole, the remainder a summation over additional isovector vector meson poles.

The VMD model of ref. [22] focused more on fitting the space-like nucleon form factors. It was found sufficient to use 3 additional vector meson poles, two of which are chosen to be the physical particles $\rho(1450)$ and $\rho(1700)$ and denoted as ρ'' and ρ''' . In Ref. [16], which extends the scenario to include time-like data, the third pole is left adjustable to compensate for the neglect of higher mass continuum like $N\bar{N}$. The pole mass was determined to be $M_{\rho'} = 1.4035 \text{ GeV}$, in association with fixing $\Lambda^2 = 12 \text{ GeV}^2$ and $Q_1^2 = 0.35 \text{ GeV}^2$ in Eq. (35). The parameters in Eq. (36) remain unaffected in both fits. Besides the fictitious ρ' , one special feature of the model is to utilize the freedom in insufficient knowledge of ρ'' and ρ''' widths and couplings, which are taken as fit parameters. Thus only the $\rho(770)$ is isolated from the

TABLE I. The relevant poles (M_v in GeV) and the corresponding residues that enter the summation in Eq. (34).

$M_{\rho'} = 1.4035$		$M_{\rho''} = 1.45$		$M_{\rho'''} = 1.69$	
$a_1^{\rho'}$	$a_2^{\rho'}$	$a_1^{\rho''}$	$a_2^{\rho''}$	$a_1^{\rho'''}$	$a_2^{\rho'''}$
-9.913	-4.731	13.01	0.263	-3.497	2.947

summation so that $\tilde{F}_i^\rho(t)$ contains no parameters that need to be determined.

With a_i^v taken as parameters, Eq. (20), i.e. PQCD power counting, can be achieved by *choosing* the residues a_i^v of the vector meson poles such that the leading coefficients in the $1/t$ expansion cancel. This is what the use of a single ρ -pole can never achieve, since further excited states are needed for such cancellation. This also means that one has only an effective *model* since the dynamical parameters for $\rho(1450)$ and $\rho(1700)$ would likely not correspond to physical ones. We summarize in Table I the relevant meson poles and the corresponding residues of the higher excited states given by Table 1 of Ref. [16] (only the so-called “Fit 2” is needed).

The parametrization agrees with experiment quite well up to $t \sim 6 \text{ GeV}^2$, beyond which it overruns data because of the choice of low Λ in the logarithmic factor $L(t)$. This is in contrast with the empirical fit of Eq. (21). It arises in part because the VMD model focuses more on the spacelike region where one has more data, but is of less concern to us. In order to conform to experiment for larger timelike momentum transfer, however, a modification of the $L(t)$ factor is needed. The empirical fit of Eq. (21) suggests a convenient modification

$$L(t) = \begin{cases} \left[\ln \left(\frac{\Lambda^2 - t}{Q_1^2} \right) \right]^{-\gamma} & \text{for } t \leq \frac{\Lambda^2}{2} - \Delta, \\ -\frac{1}{2\Delta} L' \left(\frac{\Lambda^2}{2} - \Delta \right) \left(t - \frac{\Lambda^2}{2} \right)^2 + H(\Delta) & \text{for } |t - \frac{\Lambda^2}{2}| < \Delta, \\ \left[\ln \left(\frac{t}{Q_1^2} \right) \right]^{-\gamma} & \text{for } t \geq \frac{\Lambda^2}{2} + \Delta. \end{cases}$$

where we match a parabola between the interval $\frac{\Lambda^2}{2} - \Delta < t < \frac{\Lambda^2}{2} + \Delta$ by tuning the constant $H(\Delta)$. Note that $-L'(\Lambda^2/2 - \Delta) = L'(\Lambda^2/2 + \Delta)$ and $L(\Lambda^2/2 - \Delta) = L(\Lambda^2/2 + \Delta)$, or $L(t)$ is symmetric with respect to $t = \Lambda^2/2$. To smooth out the artificial rise that occurs beyond $t \sim 6 \text{ GeV}^2 = \Lambda^2/2$ for the original fit, we choose $\Delta = 0.5 \text{ GeV}^2$ and $H(\Delta) \sim 0.10279$.

Fig. 6 shows the resulting VMD-based proton magnetic form factor for both space-like and time-like t , with the modified log factor in the time-like region, where the result is plotted in more detail in Fig. 2. We see that the trend of the proton data can be described by this model. In contrast, from Fig. 3, where the extension of the VMD result to neutron case is given, there is a significant deviation from G_M^n data, signaling the incapability

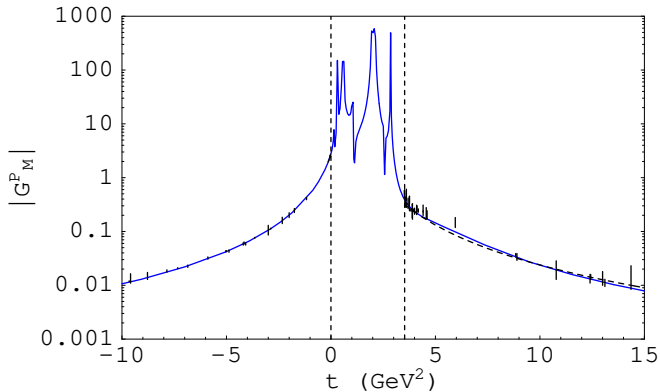


FIG. 6. The VMD-based proton magnetic form factor with the modified logarithmic factor. The unphysical region is marked by two vertical lines. The dash-line in the time-like region represents a fit with $C = 53$ in Eq. (21).

of the three-plus-one pole fit to describe the neutron data consistently. This fact was admitted to in Ref. [16].

One useful aspect of a dispersion approach is that analyticity can help determine the signs of the time-like form factors from space-like region. Unlike Eqs. (22) and (23) where the signs are put in by hand, it is more natural in the dispersion analysis since all the time-like information can in principle be obtained via the dispersion relation in Eq. (31), where the spectral function $\text{Im} F(t)$ is analytically continued from the space-like region. One can readily check this by finding out the value of the magnetic form factors from the VMD analysis at threshold: $G_M^p(4m_N^2) \cong +0.39$ while $G_M^n(4m_N^2) \cong -0.22$. From both Figs. 2 and 3, since neither G_M^p nor G_M^n seem to cross the t -axis, G_M^p remains positive while G_M^n remains negative throughout the timelike region. VMD analysis thus gives G_M^p and G_M^n with a relative sign.

B. $B^0 \rightarrow D^{*-} p \bar{n}$ in VMD Approach

We calculate the branching fraction of $B^0 \rightarrow D^{*-} p \bar{n}$ through the vector portion of the charged weak current in the VMD model, again taking a_1 as extracted from $B^0 \rightarrow D^{*-} \rho^+$. The results for $B^0 \rightarrow D^{*-} p \bar{n}$ are,

$$\text{Br}_V^{\text{LF}} = (1.69 \times 10^{-4}) \left(\frac{a_1}{0.74} \right)^2, \quad (37)$$

$$\text{Br}_V^{\text{BSW}} = (2.06 \times 10^{-4}) \left(\frac{a_1}{0.86} \right)^2, \quad (38)$$

which are respectively about 12% and 14% of the experimental value of $(14.5_{-3.0}^{+3.4} \pm 2.7) \times 10^{-4}$. Varying pole masses slightly does not drastically modify the result. The differential decay rate is plotted in Fig. 4, where one sees that it peaks not far above the $p \bar{n}$ threshold of $t \sim 3.53 \text{ GeV}^2$. The contribution from the region of $3.53 < t < 6 \text{ GeV}^2$ is more than 80% of the total rate

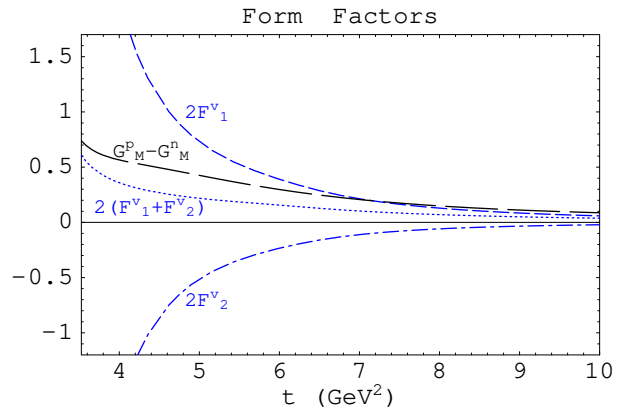


FIG. 7. $G_M^p - G_M^n$ (long-dashed) from our fit to nucleon form factor data compared with $2F_1^v + 2F_2^v (= G_M^p - G_M^n)$, dotted) from the VMD analysis, for the kinematically allowed region of t in $B^0 \rightarrow D^{*-} p \bar{n}$. Also shown are $2F_1^v$ (short-dashed) and $2F_2^v$ (dot-dashed) from the VMD model.

for both LF and BSW models. Had we used Eq. (35), because of the artificial rise in this original logarithmic factor, the contribution from $t > 6 \text{ GeV}^2$ ($m_{p \bar{n}} > 2.45 \text{ GeV}$) would be ~ 2.5 times higher. The contribution from $t < 6 \text{ GeV}^2$, however, is unchanged.

It is clear that the branching fractions obtained in the VMD approach of Ref. [16] are typically 5 times smaller than our phenomenological model discussed in the previous section. This can be simply traced to the inadequacy in accounting for neutron data by the VMD model, as seen by comparing Figs. 2 and 3. While giving a reasonable fit in the proton case, the absolute value of its neutron form factor is simply below all data points. The VMD model was tuned more on the proton where data is much more abundant. Since the proton and neutron magnetic form factors are opposite in sign, if the VMD approach is improved to give better account of $|G_M^n|$ data, the combination $G_M^p - G_M^n$ would increase.

IV. DISCUSSION AND APPLICATIONS

A. Nucleon Form Factor Decompositions

We plot various form factor combinations in Fig. 7. The long dashed line shows $G_M^p - G_M^n = 2(F_1^v + F_2^v)$ from our phenomenological fit, which assumes G_M^p and G_M^n have opposite sign. As discussed in the previous section, because the VMD model gives much lower value for $|G_M^n|$, $G_M^p - G_M^n$ in the VMD model (denoted as dotted line and labeled by $2(F_1^v + F_2^v)$) stays below the phenomenological model. However, had we chosen the proton and neutron form factors to be of the same sign, $G_M^p - G_M^n$ for our phenomenological fit would be very close to the solid line which is the t -axis, and would give a rate that is two orders of magnitude too small.

TABLE II. Comparison of nucleon form factor decompositions. The fraction $\mathcal{R}_X \equiv \mathcal{B}_X/\text{Br}_V$ are defined in text, where X stands for any combination of F_1 , F_2 or their product.

	$\mathcal{R}_{(F_1^v+F_2^v)}$	$\mathcal{R}_{F_2^v}$	$\mathcal{R}_{(F_1^v+F_2^v)\cdot F_2^v}$
LF/BSW	1.3	0.24	-0.54
	$\mathcal{R}_{F_1^v}$	$\mathcal{R}_{F_2^v}$	$\mathcal{R}_{F_1^v\cdot F_2^v}$
LF/BSW	26.00	18.25	-43.25

Besides helping to fix the sign of G_M^n by analyticity, another utility of discussing the VMD approach is that it can give some insight to the F_2 nucleon form factor. Because of lack of experimental information, we have dropped the F_2 contribution in our phenomenological approach, and we need to check the validity of this. The weak vector current induced decay amplitude, upon squaring, can be expressed as

$$|\mathcal{M}_V|^2 = |\mathcal{M}_{F_1+F_2}|^2 + |\mathcal{M}_{F_2}|^2 + 2\text{Re}(\mathcal{M}_{F_1+F_2}\mathcal{M}_{F_2}^*) \quad (39)$$

where $\mathcal{M}_{F_1+F_2, F_2}$ denote $F_1^v + F_2^v$, F_2^v terms in Eq. (17). Decomposing $\text{Br}_V = \mathcal{B}_{F_1+F_2} + \mathcal{B}_{F_2} + \mathcal{B}_{(F_1+F_2)F_2}$ where the last term is the interference term, we define the relative fractions such as $\mathcal{R}_{(F_1+F_2)} \equiv \mathcal{B}_{(F_1+F_2)}/\text{Br}_V$ from $(F_1^v + F_2^v)$ alone. We find $\mathcal{R}_{(F_1+F_2)}$, \mathcal{R}_{F_2} , $\mathcal{R}_{(F_1+F_2)\cdot F_2} = 130\%$, 24% , -54% (Table II) in the VMD model, for both LF and BSW $B^0 \rightarrow D^*$ form factor models. Note that the $2(F_1^v + F_2^v) = G_M^p - G_M^n$ term gives the dominant contribution, which supports the approximation used in Sec. II. The F_2^v contribution is much smaller even though $|F_2^v(t)|$ is greater than $|F_1^v + F_2^v|$ for $t < 5 \text{ GeV}^2$, as shown by the dot-dash curve in Fig. 7. The interference term contributes $\sim 40\%$ of the $F_1^v + F_2^v$ contribution. The destructive nature is due to the relative sign between $F_1^v + F_2^v$ and F_2^v , which reduces the combined effect of the last two terms in Eq. (39).

It is instructive to compare with Eq. (8), where one decomposes into F_1 and F_2 directly. As shown in Table II, the individual terms from this decomposition are an order of magnitude larger, and only after strong cancellations does one arrive at Br_V . It is therefore not a very useful decomposition. We see from Fig. 7 that the magnitudes of F_1^v and F_2^v are all greater than their sum, hence $F_1^v + F_2^v$ together with F_2^v is a better decomposition for t close to threshold, which is what we used in our phenomenological study.

B. Prediction for $B \rightarrow D^{(*)}p\bar{n}$ Modes

Our phenomenological approach can be applied to the modes of $B^+ \rightarrow \bar{D}^{(*)0}p\bar{n}$ and $B^0 \rightarrow D^-p\bar{n}$. We show in Table III the results based on the vector current with the $B^0 \rightarrow D^{*-}p\bar{n}$ mode included for comparison. The

TABLE III. Branching fractions of the $B \rightarrow \bar{D}^{(*)}p\bar{n}$ modes from the vector current, obtained by using the phenomenological form factors with $|G_M^p| = |G_E^p|$ and $|G_M^n| = |G_E^n|$ ($|G_E^n| = 0$) for the first (second) set.

	$\text{Br}_V \times 10^4$		$\text{Br}_V \times 10^4$	
	$ G_M^n = G_E^n $		$ G_E^n = 0$	
	LF	BSW	LF	BSW
$B^0 \rightarrow D^{*-}p\bar{n}$	$7.14^{+0.69}_{-0.65}$	$8.72^{+0.85}_{-0.79}$	$8.96^{+1.02}_{-0.94}$	$10.94^{+1.25}_{-1.15}$
$B^+ \rightarrow \bar{D}^{*0}p\bar{n}$	$7.64^{+0.74}_{-0.69}$	$9.33^{+0.90}_{-0.85}$	$9.59^{+1.10}_{-1.01}$	$11.71^{+1.33}_{-1.23}$
$B^+ \rightarrow \bar{D}^0p\bar{n}$	$3.92^{+0.39}_{-0.35}$	$3.21^{+0.32}_{-0.28}$	$4.89^{+0.58}_{-0.51}$	$4.00^{+0.47}_{-0.42}$
$B^0 \rightarrow D^-p\bar{n}$	$3.66^{+0.36}_{-0.32}$	$2.99^{+0.30}_{-0.26}$	$4.56^{+0.54}_{-0.48}$	$3.73^{+0.44}_{-0.39}$

differential decay rates for the other three $B \rightarrow D^{(*)}p\bar{n}$ decays are given in Fig. 8. We have used the central values of the effective coefficients that are extracted from the two-body modes [23] $\bar{B}^0 \rightarrow D^{*+}\rho^-$, $D^+\rho^-$ with values $a_1^{LF(BSW)} = 0.74 \pm 0.18 \pm 0.06$ ($0.86 \pm 0.21 \pm 0.07$) and $a_1^{LF(BSW)} = 0.89 \pm 0.08 \pm 0.07$ ($0.91 \pm 0.08 \pm 0.07$) respectively. We note that the \bar{D}^* modes in Table III are close in rate, and likewise for \bar{D} modes, which is easy to understand because of simple replacement of spectator quark in $B \rightarrow \bar{D}^{(*)}$ transition.

Although only the contribution from the weak vector current can so far be calculated, we can estimate the values of these other baryonic modes by following the recipe of Sec. II. Inspection of Table III shows that the ratio of $\text{Br}_V(B^+ \rightarrow \bar{D}^{*0}p\bar{n})/\text{Br}_V(B^0 \rightarrow \bar{D}^{*-}p\bar{n})$ remains fixed regardless of $B \rightarrow \bar{D}^*$ form factor models. Assuming similar behavior for axial contribution, we expect the $B^+ \rightarrow \bar{D}^{*0}p\bar{n}$ branching fraction to be scaled by the same factor and find the value of $\sim 15.5 \times 10^{-4}$ that is only slightly larger than the $B^0 \rightarrow D^{*-}p\bar{n}$ mode, as

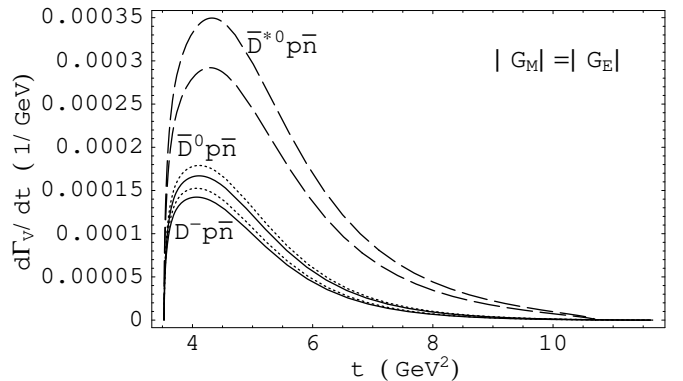


FIG. 8. The differential decay rates arising from nucleon vector current. Upper (lower) dashed line is for $B^0 \rightarrow \bar{D}^{*0}p\bar{n}$ with the BSW (LF) hadronic form factors; upper (lower) dotted and solid lines are for the $B^0 \rightarrow \bar{D}^0p\bar{n}$ and $B^0 \rightarrow D^-p\bar{n}$ modes using the LF (BSW) model.

TABLE IV. Branching fractions estimated by scaling $\text{Br}_V(B \rightarrow D^{(*)}p\bar{n})/\text{Br}_V(B^0 \rightarrow D^{*-}p\bar{n})$ of Table III with respect to the $\text{Br}(B^0 \rightarrow D^{*-}p\bar{n})$ experimental central value of 14.5×10^{-4} (Eq. (1)).

	$\text{Br} \times 10^4$		$\text{Br} \times 10^4$	
	$ G_M^n = G_E^n $		$ G_E^n = 0$	
	LF	BSW	LF	BSW
$B^+ \rightarrow \bar{D}^{*0}p\bar{n}$	15.52	15.51	15.52	15.51
$B^+ \rightarrow \bar{D}^0p\bar{n}$	7.97	5.34	7.92	5.30
$B^0 \rightarrow D^-p\bar{n}$	7.43	4.98	7.38	4.94

given in Table IV. The predicted branching fractions for $B^+ \rightarrow \bar{D}^0p\bar{n}$ and $B^0 \rightarrow D^-p\bar{n}$ from the same ansatz are in general are 2–3 times smaller. Since one is comparing $B \rightarrow \bar{D}$ vs. $B \rightarrow \bar{D}^*$, there is stronger model dependence on the transition form factor.

One can see from both Tables III and IV as well as Fig. 8 that the LF results are generally larger than the BSW ones for $B \rightarrow \bar{D}$ modes, but the case is reversed for the $B \rightarrow \bar{D}^*$ modes. This can be understood from the differences in a_1 and hadronic form factors of the LF and BSW cases. For the $B \rightarrow \bar{D}$ modes, the only hadronic form factor involved is F_1^{BD} , which behaves as a dipole and monopole in the LF and BSW models, respectively. This leads to $F_1^{LF}(t) > F_1^{BSW}(t)$ in the physical timelike region while $a_1^{LF} \cong a_1^{BSW} \cong 0.9$, giving a larger Br_V^{LF} . In contrast, for $B \rightarrow \bar{D}^*$ modes, although the dominant hadronic form factor $A_1^{LF} > A_1^{BSW}$ in the physical timelike region, it behaves as monopole for both LF and BSW models, hence the difference between A_1^{LF} and A_1^{BSW} is not as large as the previous case. However, $a_1^{LF} \sim 0.74 < a_1^{BSW} \sim 0.86$ hence we have the opposite result that BSW rates are bigger.

C. Predictions for $B^0 \rightarrow D^{*-} + \text{Strange Baryons}$

Our phenomenological approach can be extended to B^0 decay into D^{*-} plus baryon pairs containing strangeness. Recall that in Sec. II we utilized SU(2) symmetry to obtain the relation $F_{1,2}^W = F_{1,2}^p - F_{1,2}^n$ for the $p\bar{n}$ mode. In the SU(3) limit we can [24] extend this relation to modes containing strange baryons. Starting from Eq. (8), denoting $F_{1,2}^W(\mathbf{B}_s \bar{\mathbf{B}}_s')$ as the weak form factor that appears in the matrix element $\langle \mathbf{B}_s \bar{\mathbf{B}}_s' | V_\mu^+ | 0 \rangle$, we find

$$\begin{aligned}
 F_{1,2}^W(\Sigma^{+,0}\bar{\Sigma}^{0,-}) &= \mp\sqrt{2} \left(F_{1,2}^p(t) + \frac{1}{2} F_{1,2}^n(t) \right), \\
 F_{1,2}^W(\Xi^0\bar{\Xi}^-) &= F_{1,2}^p(t) + 2 F_{1,2}^n(t), \\
 F_{1,2}^W(\Sigma^+\bar{\Lambda}) &= -\sqrt{\frac{3}{2}} F_{1,2}^n(t).
 \end{aligned} \tag{40}$$

These relations enable us to calculate the contributions from the vector currents to the strange baryonic modes.

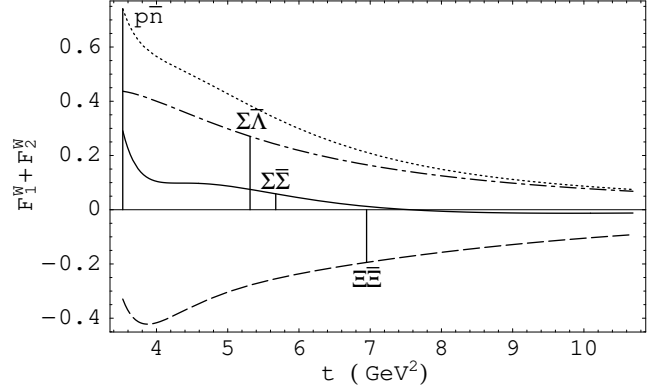


FIG. 9. $F_1^W + F_2^W$ for the $p\bar{n}$ (dotted), $\Sigma^0\bar{\Sigma}^-$ (solid), $\Xi^0\bar{\Xi}^-$ (dashed) and $\Sigma^+\bar{\Lambda}$ (dot-dashed) modes, respectively. The vertical lines specify the thresholds for the baryonic pairs.

We shall only give results from the phenomenological approach with $|G_E^n| = |G_M^n|$.

The strange baryon modes all have rates smaller than that of the $p\bar{n}$ mode due to the following reason. In Fig. 9 we plot the form factor combination $F_1^W + F_2^W = 2(F_1^v + F_2^v)$ of Eq. (17). One can see that the largest value is at the $p\bar{n}$ threshold, while for the strange baryonic modes the corresponding threshold values are all smaller. Reading off from Fig. 9, it is clear that the $\Sigma^+\bar{\Lambda}$ mode would be the dominant strange baryonic mode, with the two $\Sigma\bar{\Sigma}$ modes the smallest. This is shown in Fig. 10 for the differential decay rates using LF mesonic form factors, and the total decay rates given in Table V. Note that the differential decay rate for the $D^{*-}\Sigma\bar{\Sigma}$ mode has a zero at $t \sim 7.5 \text{ GeV}^2$ because $F_1^W(\Sigma\bar{\Sigma}) + F_2^W(\Sigma\bar{\Sigma})$ changes sign, as can be seen from Fig. 9.

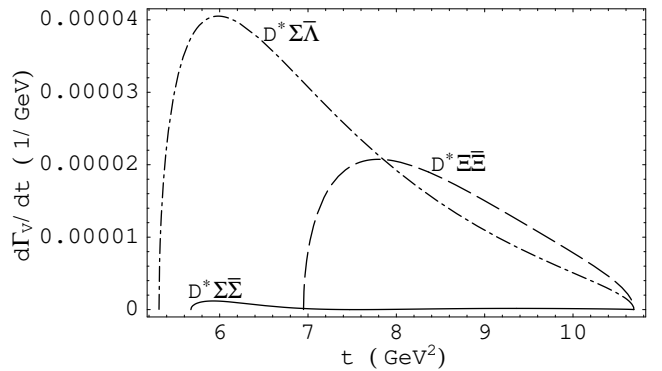


FIG. 10. Differential rates of $B^0 \rightarrow D^{*-}\Sigma^+\bar{\Lambda}$ (dot-dashed), $D^{*-}\Xi^0\bar{\Xi}^-$ (dashed) and $D^{*-}\Sigma^+\bar{\Sigma}^0$ (solid) from the phenomenological model, with LF hadronic form factors.

TABLE V. Branching fractions for $B^0 \rightarrow D^{*-} +$ strange baryon pairs from vector current using the phenomenological G_M form factors of Sec. II assuming $|G_E^n| = |G_M^n|$.

	$\text{Br}_V^{\text{LF}} \times 10^4$	$\text{Br}_V^{\text{BSW}} \times 10^4$
$B^0 \rightarrow D^{*-} p\bar{n}$	7.19	8.78
$B^0 \rightarrow D^{*-} \Sigma^+ \bar{\Lambda}$	1.09	1.38
$B^0 \rightarrow D^{*-} \Xi^0 \bar{\Xi}^-$	0.52	0.66
$B^0 \rightarrow D^{*-} \Sigma^+ \bar{\Sigma}^0$	0.01	0.02
$B^0 \rightarrow D^{*-} \Sigma^0 \bar{\Sigma}^-$	0.01	0.02

V. CONCLUSION

The main result of this paper is an attempt to account for CLEO's result on $B^0 \rightarrow D^{*-} p\bar{n}$. In a factorization approach, the nucleon pair is viewed as produced directly from the weak current. We then use an isospin relation of weak and em vector currents to obtain the vector weak nucleon form factors directly from their em partners, where a relatively large database exists. It is interesting that we can account for $\sim 60\%$ of the observed $\text{Br}(B^0 \rightarrow D^{*-} p\bar{n})$ rate in this way. A VMD model that attempts at fitting nucleon form factor data was discussed to clarify certain issues.

Interference of the weak vector current induced amplitude with the amplitude induced by the weak axial current does not manifest itself in the total rate. The latter is a simple sum of the absolute squares of both vector and axial vector. A rough estimate of axial vector contribution, together with the dominant vector contribution, seem to fit the measured rate. However, for a more reliable calculation, more measurements on time-like region $G_E^{p,n}$ and g_A are urged.

We apply our analysis to $B^+ \rightarrow \bar{D}^{(*)0} p\bar{n}$ and $B^0 \rightarrow D^- p\bar{n}$ modes to get the rates arising from the vector current. We find $\text{Br}(B^+ \rightarrow \bar{D}^{*0} p\bar{n}) \sim \text{Br}(B^0 \rightarrow D^{*-} p\bar{n})$ and $\text{Br}(B^+ \rightarrow \bar{D}^0 p\bar{n}) \sim \text{Br}(B^0 \rightarrow D^- p\bar{n})$, with the latter modes having smaller rates slightly below the 10^{-3} level. Our analysis is also applied to baryonic modes that contain strangeness. The estimated branching fractions are generally lower than the $p\bar{n}$ mode due to smaller couplings and higher thresholds. The largest modes, $B^0 \rightarrow D^{*-} \Sigma^+ \bar{\Lambda}$, is predicted at the 1×10^{-4} level.

For the analogous picture of $B \rightarrow \eta' \bar{\Lambda} p$, $\gamma \bar{\Lambda} p$ as descending from $B \rightarrow \eta' K$ and $K^* \gamma$ via $K^{(*)}$ exchange, the baryon pairs are not produced by the W boson, and it seems that the approach used here cannot be readily applied. However, some experience obtained may still be valuable. For example, in the VMD approach to $B \rightarrow \bar{D}^* p\bar{n}$, more than one pole and cancellations among them are required to reproduce the QCD predicted asymptotic behavior. For the charmless cases, the baryon pairs are no longer produced by the charged current. Instead, the $K^{(*)}$ resonances that correspond to $\rho^{','',''}$ in VMD approach, appear more as string excita-

tions. They need not obey the same QCD power countings, and perhaps may result in larger rates.

Finally, it is of great interest to estimate the rate of the charmless baryonic mode $B^0 \rightarrow \rho^- p\bar{n}$ by replacing D^{*-} in the Feynman diagram depicted in Fig. 1(b) with ρ^- . Since this is a tree-dominant mode, extending from the study presented in this paper, $\text{Br}(B^0 \rightarrow \rho^- p\bar{n})$ could be as large as that of the two-body mode $B^0 \rightarrow \rho^- \rho^+$, analogous to the relative strength of $\text{Br}(B^0 \rightarrow D^{*-} p\bar{n})$ vs $\text{Br}(B^0 \rightarrow D^{*-} \rho^+)$. Estimating via $\text{Br}(B^0 \rightarrow \rho^- p\bar{n}) \sim \text{Br}(B^0 \rightarrow \rho^- \rho^+) \times \text{Br}(B^0 \rightarrow D^{*-} p\bar{n}) / \text{Br}(B^0 \rightarrow D^{*-} \rho^+)$. From $\text{Br}(B^0 \rightarrow \rho^- \rho^+) \sim (20-40) \times 10^{-6}$ [17,25] we get $\text{Br}(B^0 \rightarrow \rho^- p\bar{n}) \sim (0.4-0.8) \times 10^{-5}$. Alternatively, we can scale from $B \rightarrow \bar{D}^* p\bar{n}$ by $|V_{ub}/V_{cd}|^2$ and phase space, decay constant etc., and again find $B \rightarrow \rho^- p\bar{n}$ at 10^{-5} order. Charmless decays are of great current interest. A more detailed discussion of $B \rightarrow \rho p\bar{n}$ modes is given elsewhere [26].

ACKNOWLEDGMENTS

We thank S. J. Brodsky for illuminating discussions and useful suggestions. This work is supported in part by the National Science Council of R.O.C. under Grants NSC-89-2112-M-002-063, NSC-89-2811-M-002-0086 and NSC-89-2112-M-002-062, the MOE CosPA Project, and the BCP Topical Program of NCTS.

-
- [1] I. Dunietz, Phys. Rev. D **58**, 094010 (1998) [hep-ph/9805287].
 - [2] S. Anderson *et al.* [CLEO Collaboration], Phys. Rev. Lett. **86**, 2732 (2001) [hep-ex/0009011].
 - [3] D. E. Groom *et al.* [Particle Data Group Collaboration], Eur. Phys. J. C **15**, 1 (2000).
 - [4] W. S. Hou and A. Soni, Phys. Rev. Lett. **86**, 4247 (2001) [hep-ph/0008079].
 - [5] T. E. Browder *et al.* [CLEO Collaboration], Phys. Rev. Lett. **81**, 1786 (1998) [hep-ex/9804018].
 - [6] C. H. Berger *et al.*, Phys. Lett. B **35**, 87 (1971); W. Bartel *et al.*, Phys. Lett. B **33**, 245 (1970); T. Jansens *et al.*, Phys. Rev. **142**, 922 (1965); G. Höhler *et al.*, Nucl. Phys. B **114**, 505 (1976); F. Borkowski *et al.*, Nucl. Phys. B **93**, 461 (1975); R. Arnold *et al.*, Phys. Rev. Lett. **57**, 174 (1986); R. C. Walker *et al.*, Phys. Lett. B **234**, 353 (1989).
 - [7] M. Ambrogiani *et al.* [E835 Collaboration], Phys. Rev. D **60**, 032002 (1999).
 - [8] A. Antonelli *et al.*, Nucl. Phys. B **517**, 3 (1998).
 - [9] T. A. Armstrong *et al.*, Phys. Rev. Lett. **70**, 1212 (1993).
 - [10] M. Castellano *et al.*, Nuovo Cim. A **14**, 1 (1973). G. Bassompierre *et al.*, Phys. Lett. B **68**, 477 (1977), Nuovo Cim. A **73**, 347 (1983); B. Delcourt *et al.*, Phys. Lett. B **86**, 395 (1979); D. Bisello *et al.*, Nucl. Phys. B **224**, 379

- (1983); Z. Phys. C **48**, 23 (1990); G. Bardin *et al.*, Phys. Lett. B **255**, 149 (1991); B **257**, 514 (1991); Nucl. Phys. B **411**, 3 (1994); (1993); A. Antonelli *et al.*, Phys. Lett. B **334**, 431 (1994); B **313**, 283 (1993).
- [11] S. J. Brodsky and G. R. Farrar, Phys. Rev. D **11**, 1309 (1975).
- [12] A. A. Logunov, N. Van Hieu and I. T. Todorov, Ann. Phys. **31**, 203 (1965).
- [13] V. A. Matveev, R. M. Muradyan and A. N. Tavkhelidze, Lett. Nuovo Cimento **7**, 719 (1973).
- [14] V. L. Chernyak and I. R. Zhitnitsky, Nucl. Phys. B **246**, 52 (1984).
- [15] R. Baldini, S. Dubnicka, P. Gauzzi, S. Pacetti, E. Pasqualucci and Y. Srivastava, Eur. Phys. J. C **11**, 709 (1999).
- [16] H. W. Hammer, U.-G. Meissner and D. Drechsel, Phys. Lett. B **385**, 343 (1996) [hep-ph/9604294].
- [17] A. Ali, G. Kramer and C. D. Lu, Phys. Rev. D **58**, 094009 (1998) [hep-ph/9804363].
- [18] M. Wirbel, B. Stech and M. Bauer, Z. Phys. C **29**, 637 (1985).
- [19] M. Bauer, B. Stech and M. Wirbel, Z. Phys. C **34**, 103 (1987).
- [20] H. Y. Cheng, C. Y. Cheung and C. W. Hwang, Phys. Rev. D **55**, 1559 (1997) [hep-ph/9607332].
- [21] A. Liesenfeld *et al.* [A1 Collaboration], Phys. Lett. B **468**, 19 (1999) [nucl-ex/9911003].
- [22] P. Mergell, U.-G. Meissner and D. Drechsel, Nucl. Phys. A **596**, 367 (1996) [hep-ph/9506375].
- [23] H. Y. Cheng and K. C. Yang, Phys. Rev. D **59**, 092004 (1999) [hep-ph/9811249].
- [24] See, for example, H. Georgi, *Weak Interactions And Modern Particle Theory*, Benjamin/Cummings, 1984.
- [25] W. S. Hou and K. C. Yang, Phys. Rev. D **61**, 073014 (2000) [hep-ph/9908202].
- [26] C. K. Chua, W. S. Hou and S. Y. Tsai, hep-ph/0108068.